Available online at www.sciencedirect.com
SCIENCE DIRECT®
Solid State Sciences 6 (2004) 15–20
Solid State Sciences
www.elsevier.com/locate/ssscie

DFT calculations on the electronic structure of $CuTe_2$ and Cu_7Te_4

S.F. Matar [a,*], R. Weihrich [a,b], D. Kurowski [b], A. Pfitzner [b]

[a] *Institut de chimie de la matière condensée de Bordeaux, ICMCB, CNRS, Université Bordeaux 1, 87, avenue du docteur Albert Schweitzer, 33608, Pessac cedex, France*

[b] *Institut für Anorganische Chemie, Universtität Regensburg, Universitätsstraße 31, 93040 Regensburg, Germany*

Received 8 July 2003; accepted 8 September 2003

Abstract

The electronic structures of $CuTe_2$ and Cu_7Te_4 were determined from first principles. The band structures, densities of states and projected contributions of atomic states were calculated with DFT ASW- and FP-LAPW codes. Both compounds stabilize by establishing metallic instead of ionic systems. This behaviour is explained in terms of partly occupied valence bands that result from a range of Cu–Te, Cu–Cu and Te–Te bonding. As a consequence the Cu–d states show contributions to the valence states, while their maxima lie at −2 eV below the Fermi energy. In $CuTe_2$ the bonding of Te–Te–π^* and Cu–d states leads to an overlap of valence and conduction bands. Thus the character of the valence band is of Cu–e_g and Te–p character.

Keywords: Copper tellurides; Pyrite structure; DFT-LDA; Conductivity; Band and bond character; ASW-E_{COV}

1. Introduction

The relation of structures and electronic properties of solid state Cu compounds is of great interest in research not only since the discovery of high temperature superconductors [1], but also because of magnetic effects (Cu_2O [2], CuF_2 [3]) and ionic conductivity [4]. Ternary copper compounds like the chalcopyrite [5] reached a huge interest because of the combination of semiconducting behaviour and transparency. The properties of these compounds are well understood in terms of their electronic structure. At least first principle calculations within the framework of density functional theory (DFT) served as helpful methods herein [2–5,18].

By contrast we have less knowledge on the electronic structure of the heavier chalcogenides that provide a large variety of interesting structures and compositions within which $CuTe_2$ and Cu_7Te_4 serve as two interesting examples of the Te-rich and Cu-rich sides of the binary Cu–Te system [6,7].

$CuTe_2$ is a pyrite type compound (Fig. 1) and its crystal structure was recently refined on high pressure synthesized single crystals [8]. AX_2 compounds of this structure contain diatomic entities (here Te–Te) in the octahedral holes of an FCC sublattice of atom type A (here Cu). Transferring the ionic picture of pyrite (FeS_2) itself, one might expect an ionic description of "$Cu^{2+}(Te_2)^{2-}$". On the other hand, a Cu–d^9 configuration would be expected to cause a Jahn–Teller distortion [9]. As for $CuTe_2$ the pyrite type was determined by X-ray structure determination with copper appearing in an environment of cubic symmetry where only the angles slightly differ from an ideal octahedron, while the distances to the six Te neighbours are equal. The experimental observation of metallic conductivity shows the necessity to use an enhanced description of the electronic structure of $CuTe_2$. There are earlier measurements on the magnetic susceptibility, NMR and electrical resistivity of copper dichalcogenides [10]. However, the electronic structure could not be understood and the nature of valence and conduction bands are "not really known" giving three "possible schemes" for the contribution of e_g, s and/or t_{2g} electrons to the local susceptibilities on the Cu sites.

Cu_7Te_4 is also found to show metallic conductivity. It was found [11] to crystallize in a layered structure of trigonal symmetry (Fig. 2) with an inversion centre ($P\bar{3}m1$), contrary to an older publication ($P3m1$ [12]). Te atoms form a distorted hexagonal sublattice. The Te layers are connected by copper atoms in two different tetrahedral

* Corresponding author.
E-mail address: s.matar@drimm.u-bordeaux1.fr (S.F. Matar).

1293-2558/$ – see front matter
doi:10.1016/j.solidstatesciences.2003.09.012

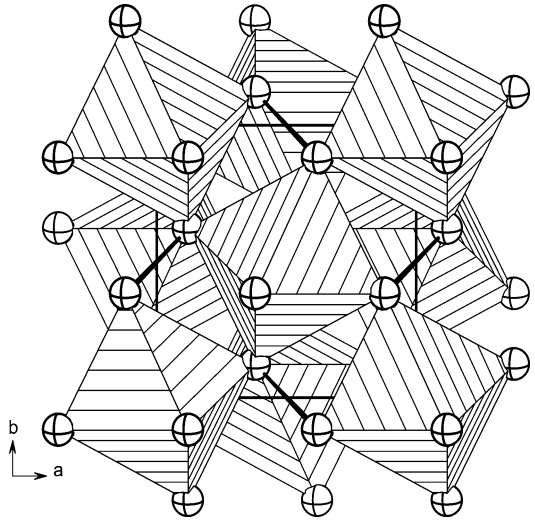

Fig. 1. Crystal structure of $CuTe_2$, the "$CuTe_6$"-octahedra and Te–Te units are highlighted.

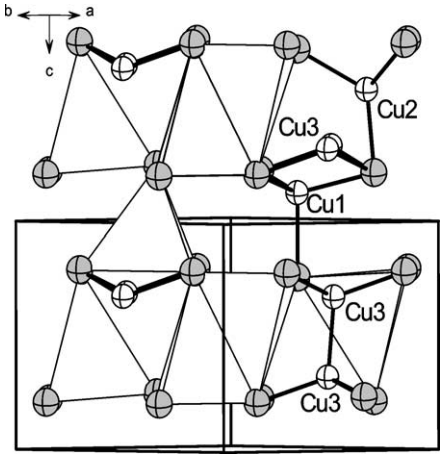

Fig. 2. Crystal structure of Cu_7Te_4, two layers connected by Cu1, filled by Cu3 and Cu2.

holes. A third Cu site within every second layer leads to an alternating copper-rich and copper-poor sandwich structure. As a consequence this Cu atom is connected to only three Te and a layered-like network of Cu–Cu and Cu–Te bonds is formed. For the Te atoms the layering results in two distinct coordination spheres. These match in the coordination by six Cu within 2.8 Å in one hemisphere, but differ within the second hemisphere where only one Te site is coordinated by a seventh Cu atom, while the other one is uncoordinated up to a distance of 3.8 Å where four Te atoms appear. From these considerations the point of interest was to investigate how the local structure and the nature of the Cu–Te and Cu–Cu bonds are represented in the electronic structure. Again, the composition does not indicate a simple ionic picture with a formal charge of $+1.25$ at the Cu site.

2. Computational details

The band structures of $CuTe_2$ and Cu_7Te_4 were calculated out within the framework of density functional theory (DFT) in its local density approximation (LDA) [13] to the electron exchange and correlation. Density of states and band structures were calculated using the accurate full potential linearized augmented plane wave (FP-LAPW) method [14]. For the exchange-correlation potential the LDA approximation was used as parametrized by Perdew and Wang [15]. Brillouin-zone integrals were approximated using the special k-point sampling of Monkhorst and Pack [16]. The difference in total energies is converged to below 0.002 eV with respect to k-point integration and kinetic energy cutoff. Therefore, the same matrix size (approximately 97 plane waves per atom) in the BZ was used in each of the total energy calculations. The k-point mesh was varied to a size of $9 \times 9 \times 9$. This was found sufficient to achieve the desired accuracy.

Further we carry out an analysis of the chemical bonding obtained from the covalent bond energy concept E_{COV} [17] implemented within the ASW method by V. Eyert [18]. Referring the reader to these publications for details, it suffices to mention here that negative E_{COV} values point to bonding states because they contribute to the stability of the system while positive E_{COV} are relevant to antibonding states. E_{COV} can be resolved for pair interactions within a crystal lattice, i.e., Cu–Te, Te–Te and Cu–Cu.

3. Results and discussion

3.1. The electronic band structure of $CuTe_2$ and Cu_7Te_4

The electronic structures of $CuTe_2$ and Cu_7Te_4 were carried out using the experimentally determined crystallographic parameters [8,11]. Searching for the electronic ground states for both compounds paramagnetic configurations were found to be the lowest in energy. That agrees with the experimental results [10]. The corresponding band structures are given in Figs. 3 and 4. One can observe that both compounds exhibit gaps above the Fermi energy. In the case of Cu_7Te_4 one can clearly observe that it just misses to be a semiconductor: The Fermi energy crosses the highest occupied bands. Counting the bands we find that one hole per formula unit is built in the conduction band. This corresponds with the previous considerations within the ionic picture, where one electron is missing to create Cu^+ and Te^{2-} ions. Another issue of interest is the highly dispersing bands at the Fermi level. The character of valence and conduction band will be shown subsequently by the site projected DOS.

$CuTe_2$ also shows highly dispersing bands crossed by the Fermi energy. A gap is indicated in the band structure at relatively high energies of $+2.5$ eV. This situation can again be described in terms of a partly filled valence band. There

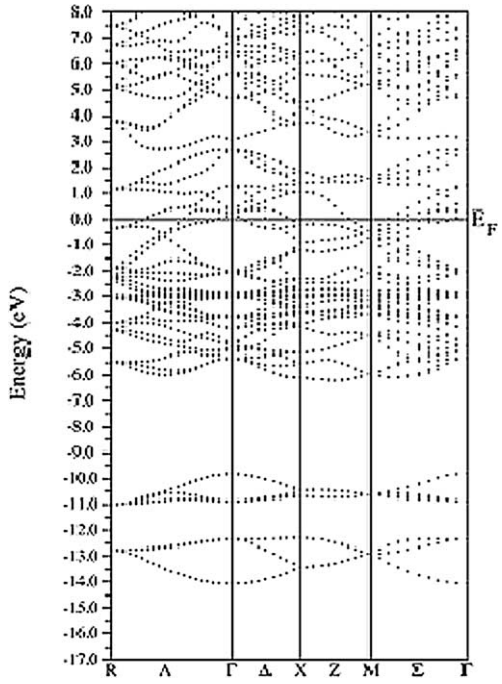

Fig. 3. Electronic band structure of $CuTe_2$ from FP-LAPW calculations.

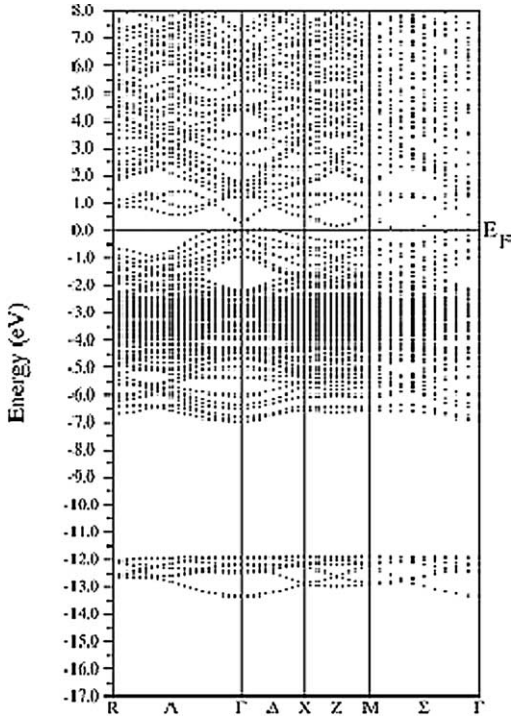

Fig. 4. Electronic band structure of Cu_7Te_4 from FP-LAPW calculations.

is a huge overlapping of band groups near the Fermi energy that can be understood by the site projected density of states.

3.2. Site projected density of states and chemical bonding properties of $CuTe_2$

We analyze the character of the bands and the main interactions Cu–Te and Te–Te by the use of site projected

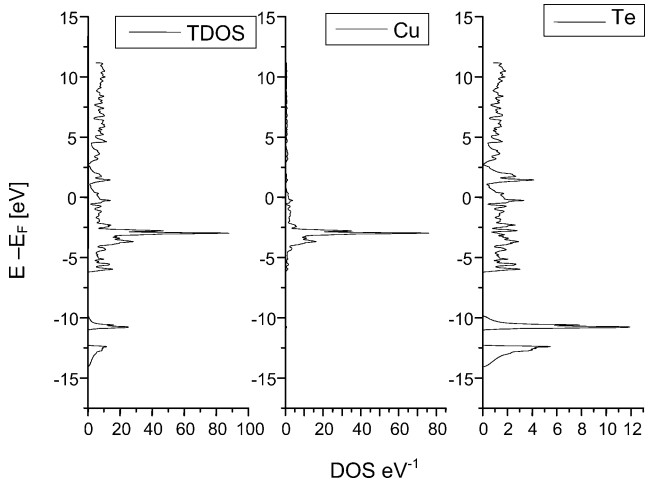

Fig. 5. Site projected density of states (PDOS) on atoms for $CuTe_2$.

DOS and the covalent bond energy concept E_{COV}. First we find the typical features of a pyrite type compound due to a molecular X–X unit. Thus the bands at -10 eV must be attributed to $\sigma^*_{s/s}$ bands, as seen in Fig. 5. They are followed by π_p, π_p and π^*_p, that would be completely filled in a $[Te_2]^{2-}$ model. This is not observed for the current calculations on $CuTe_2$, where the Fermi level crosses π^*_p-like bands. They interact with Cu–d states that lie within the same energy range. With the Cu–d maxima at -3 eV $CuTe_2$ differs from other pyrite type 3d metal disulfides (AS_2, A = Fe, Ni). For those disulfides LDA calculations predict the transition metal 3d orbitals just below the Fermi energy forming the valence band [20]. In the case of $CuTe_2$ the valence band is built by strongly mixed states. The contributions of both Cu and Te orbitals are shown in the orbital projected DOS (Fig. 6). The states at the Fermi level indicate that Cu–d orbitals are not completely filled. This is due to bonds between the transition metal-e_g and π_p states of the X_2-entity that are well-known within pyrite type compounds.

Moreover, the analysis of the AO contributions to the bands of $CuTe_2$ shows that the bands at the Fermi level are the result of bonding between copper s, p, and d states with Te–p and –d orbitals. From the E_{COV} analysis, we find Cu–Cu and Te–Te interactions to be small as compared to Cu–Te so that only the Cu–Te covalent bond energy plot within $CuTe_2$ is shown in Fig. 6(b). The E_{COV} characterizes a half bonding and half antibonding behaviour. Antibonding states at the top of the VB extend above the Fermi level. This leads to conclude that neither the Cu–d states are fully occupied nor the upper states of the $[Te_2]^{2-}$ units.

This situation was described by a depletion of metal d charge density towards the anionic neighbor and at the same time with notable back bonding via metal s and p states for alloys. The reason for this behaviour is to be found in the relative atomic orbital energies of the A and X atom. The energy difference between the highest occupied Cu and the lowest unoccupied Te orbitals is not high enough to lead to a

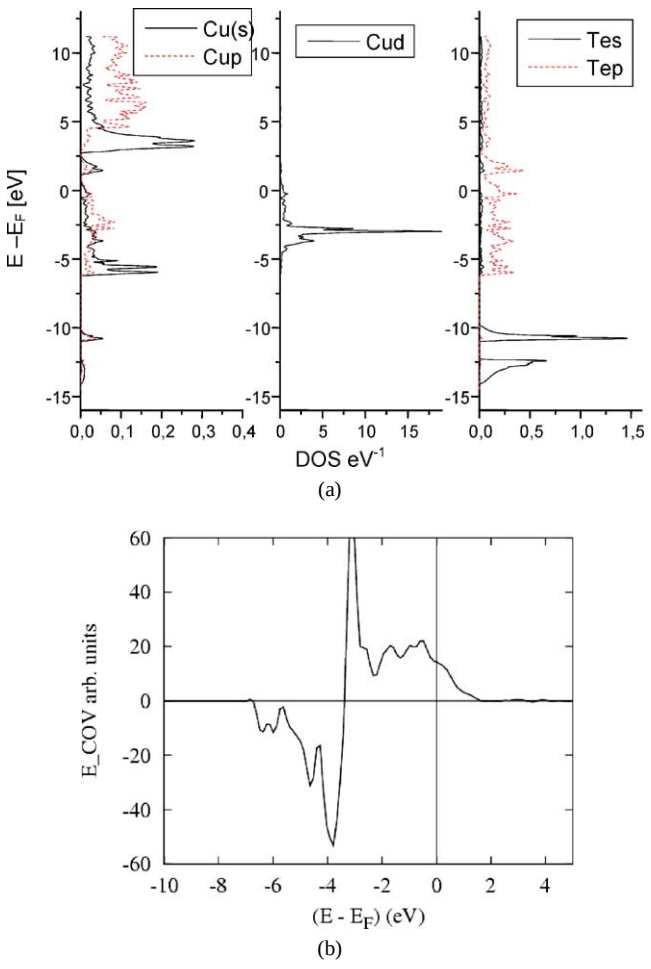

Fig. 6. (a) Site projected density of states (PDOS) on atomic orbitals for $CuTe_2$. (b) The covalent bond energy for the Cu–Te interaction accounting for all 4Cu and 8Te in the structure as obtained from ASW calculations.

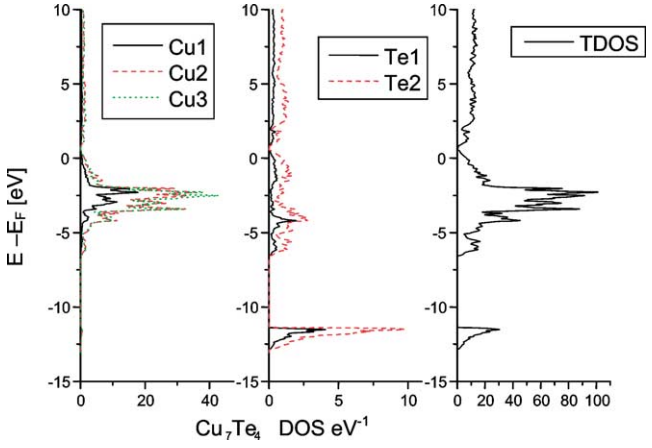

Fig. 7. Site projected density of states (PDOS) on Te atoms in Cu_7Te_4 LAPW calculations.

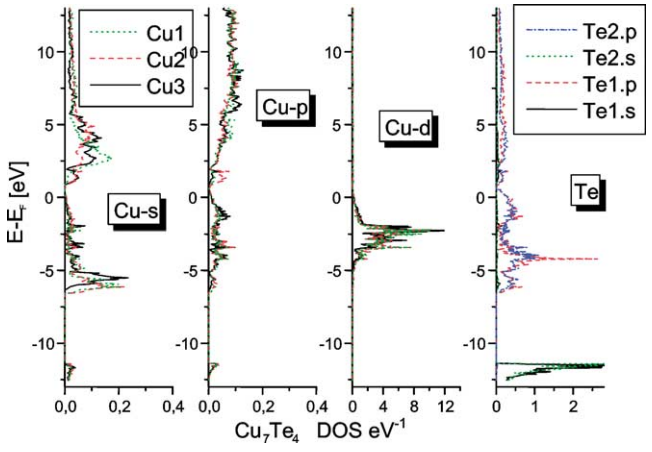

Fig. 8. Site projected density of states (PDOS) on Cu and Te atomic orbitals for Cu_7Te_4.

complete charge transfer corresponding to the ionic picture. On the contrary, the near lying energy levels enable a large degree of overlap leading to a broad valence band. That is successfully described by the electronic band structure. The situation is rather similar to that in the metallic pyrite type $AuSb_2$, where the relative energy levels of interacting orbitals lead to negatively charged Au [19,20].

3.3. Site projected density of states for Cu_7Te_4

In Cu_7Te_4 we observe a band gap at $+0.1$ eV in the calculated band structure (Fig. 4). Nevertheless, the highest occupied states cross the Fermi level, so that Cu_7Te_4 just misses to be a semiconductor. The density of states (Fig. 7) shows a different behaviour of the Cu states than in $CuTe_2$ with a larger broadening of the maxima from -5 to $+0.1$ eV and less contributions at the Fermi energy. The shape of the DOS for the different Cu sites are similar, while the distinct coordination for one Cu site (Cu1 in Fig. 7) by Te is represented in slight deviations of its density of states. The main characteristics of the DOS are due to Cu–Cu interactions and come along with the Cu–d states (Fig. 8). We observe a bonding with 4s and 4p orbitals of copper within the valence band that is very low.

The densities of states for Te indicate contributions for the entire valence band from -0.6 to $+0.1$ eV. The main difference between the two Te sites is found in the sharper peak for Te1 at -4 eV while Te2 shows less discrete but broader contributions. According to the orbital projected DOS (Fig. 8) this can be directly related to p states that point towards Cu for Te2, but act as lone pairs for Te1. The chemical bonding features can be, here too, made explicit from the covalent bond energy E_{COV} computed within the aforementioned ASW method [18]. Despite the presence of three different Cu positions we only show the Cu–Te interaction for one of them as the Cu–Cu interaction is significant in Cu_7Te_4. This is given in Fig. 9, respectively in two panels; we stress that in order to make comparisons pertinent we show the interactions atom to atom despite different site multiplicity. The Cu–Te interaction is similar to that observed in $CuTe_2$ in the sense of a half bonding (lower energy part) and half antibonding (upper energy part)

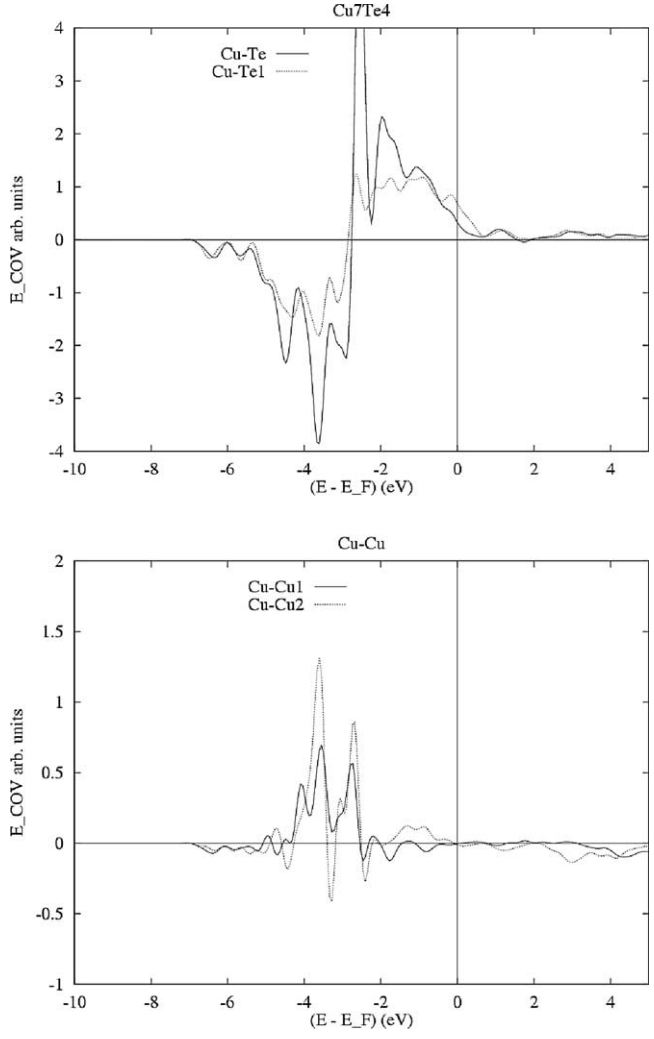

Fig. 9. Covalent bond energy of atom-to-atom interaction within Cu_7Te_4.

VB which is dominated by Cu–Te interaction extending to above the Fermi level (not fully occupied). One can notice less bonding as well as antibonding characters for the Cu–Te_1 (in-layer) as with respect to the Cu–Te interaction which prevails between layers. This can be explained by the fact that less Cu is involved in the bonding with Te within the layers and this is shown by the Cu–Cu interaction in the lower panel of Fig. 9. Regardless of which Cu position is involved, one can see that the Cu–Cu interaction is antibonding within the VB but vanishes at the Fermi level.

In summary we see the stabilization of a Cu–Te composition that is done by establishing a metallic situation. Again the stabilization is not done by a total charge transfer from Cu to Te like in an ionic compound, but by a system of huge Cu–Te and Cu–Cu interactions leading to a broad valence band that is not fully occupied. The two types of bonding contribute in their way to establish that situation: Cu–Cu interactions lead to a broadening of the Cu–d contributions over a large energy interval reaching the Fermi energy, while the Cu–Te bonds dominate near the Fermi energy. This explains the flat and broad bands previously described for the band structure.

4. Conclusion

The electronic band structures of $CuTe_2$ and Cu_7Te_4 have been investigated within density functional theory methods. Both compounds are found to be metals. While their band structures exhibit gaps above the Fermi energy they miss to be semiconductors. Characteristic for both compounds is the strong mixing of Cu–s, –p, –d and Te–p and –s states building broad bands at the Fermi level that are partially occupied. This explains the metallic behaviour and is the result of the energetically close atomic orbital levels of Cu 3d, 4sp and Te 5p that allow a strong mixing. Thus a metallic state with partially unoccupied Cu–d orbitals (d^{10-x}) is energetically preferred to a suggested ionic configuration. Both Cu–Te systems do not stabilize by establishing ionic compounds with a total charge transfer from Cu to Te but by broad, partly filled valence bands, built by large Cu–Cu, Te–Cu and Te–Te interactions.

Acknowledgements

Computational facilities of the intensive scientific pole “M3PEC”—DRIMM of the University Bordeaux 1 using the supercomputer “Regatta” are gratefully acknowledged. This work was financially supported by the Fonds der Chemischen Industrie (FCI).

References

[1] J.G. Bednorz, K.A. Müller, Z. Phys. 64 (1986) 189.
[2] E. Ruiz, S. Alvarez, P. Alemany, R.A. Evarestov, Phys. Rev. B 56 (12) (1997) 7189–7196.
[3] J.E. Jaffe, A. Zunger, Phys. Rev. B 28 (10) (1983) 5822–5847.
[4] E. Freudenthaler, A. Pfitzner, Solid State Ionics 101–103 (1997) 1053–1059.
[5] R. Reinhardt, I. de P.R. Moreira, C. de Graaf, R. Dovesi, F. Illas, Chem. Phys. Lett. 319 (2000) 625–630.
[6] R. Blachnik, M. Lasocka, U. Walbrecht, J. Solid State Chem. 48 (1983) 431.
[7] K. Van Con, H. Rodot, C. R. Acad. Sci. Paris 260 (1965) 1908.
[8] D. Kurowski, PhD thesis, University of Regensburg, Germany, 2003.
[9] M.D. Towler, R. Dovesi, V.R. Saunders, Phys. Rev. B 52 (14) (1995) 10150–10159.
[10] G. Krill, P. Panissod, M.F. Lapierre, F. Gautier, C. Robert, M. Nassr-Eddine, J. Phys. C: Solid State Phys. 9 (1976) 1521.
[11] A. Zimmerer, PhD thesis, University of Siegen, Germany, 1996.
[12] R.V. Baranova, Sov. Phys. Crystallogr. 12 (1967) 221.
[13] W. Kohn, L.J. Sham, Phys. Rev. A 140 (1965) 1133;
P. Hohenberg, W. Kohn, Phys. Rev. B 136 (1964) 864.
[14] P. Blaha, K. Schwarz, G.K.H. Madsen, D. Kvasnicka, J. Luitz, in: K. Schwarz (Ed.), WIEN2k, An Augmented Plane Wave + Local Orbitals Program for Calculating Crystal Properties, Technical University of Vienna, Vienna, 2001, ISBN 3-9501031-1-2.
[15] J.P. Perdew, Y. Wang, Phys. Rev. B 45 (1992) 13244.

[16] H.J. Monkhorst, J.D. Pack, Phys. Rev. B 13 (1976) 5188.
[17] N. Börnsen, B. Meyer, O. Grotheer, M. Fähnle, J. Phys.: Condens. Matter 11 (1999) L287.
[18] V. Eyert, Private communication on unpublished results, 2002; V. Eyert, Int. J. Quant. Chem. 77 (2000) 1007.
[19] R. Weihrich, PhD thesis, University of Regensburg, Germany, 2001.
[20] A.C. Stueckl, R. Weihrich, K.-J. Range, in: S.H. Feng, J.S. Chen (Eds.), Frontiers of Solid State Chemistry, in: Proceedings of the International Symposium on Solid State Chemistry in China, August 9–12, Changchun, China, 2002, pp. 117–124.